RESEARCH ARTICLE

Improved Visualization and Specific Binding for Metabotropic Glutamate Receptor Subtype 1 (mGluR1) Using [11C]ITMM with Ultra-High Specific Activity in Small-Animal PET

Tomoteru Yamasaki *, Masayuki Fujinaga, Joji Yui, Hidekatsu Wakizaka, Tomoyuki Ohya, Nobuki Nengaki, Masanao Ogawa, Yoko Ikoma, Akiko Hatori, Lin Xie, Kazunori Kawamura, Ming-Rong Zhang

Molucular Probe Program, Molecular Imaging Center, National Institute of Radiological Sciences, Chiba, Japan

* yamato@nirs.go.jp

Abstract

Metabotropic glutamate receptor subtype 1 (mGluR1) is a crucial target in the development of new medications to treat central nervous system (CNS) disorders. Recently, we developed N-[4-[6-(isopropylamino)pyrimidin-4-yl]-1,3-thiazol-2-yl]-4-[11C]methoxy-N-methyl-benzamide ([11C]ITMM) as a useful positron emission tomography (PET) probe for mGluR1 in clinical studies. Here, we aimed to improve visualization and threshold of specific binding for mGluR1 using [11C]ITMM with ultra-high specific activity (SA) of > 3,500 GBq/μmol in rat brains. A two-tissue compartment model indicated large differences between the two SAs in the constants k_3 and k_4, representing binding ability for mGluR1, while constants K_1 and k_2 showed no differences. The total distribution volume (V_T) values of conventional and ultra-high SA were 9.1 and 11.2 in the thalamus, 7.7 and 9.7 in the striatum, and 6.4 and 8.5 mL/cm^3 in the substantia nigra, respectively. The specific binding of [11C]ITMM with ultra-high SA was significantly higher than the conventional SA, especially in the basal ganglia. Parametric PET images scaled with V_T of the ultra-high SA clearly identified regional differences in the rat brain. In conclusion, PET studies using [11C]ITMM with ultra-high SA could sufficiently improve visualization and specific binding for mGluR1, which could help further understanding for mGluR1 functions in CNS disorders.

Introduction

Glutamate is a major neurotransmitter that triggers excitatory neurotransmission via receptor binding in the central nervous system (CNS). Two types of glutamate receptors are recognized: ionotropic and metabotropic. Metabotropic glutamate receptors (mGluRs) are G-protein-

coupled receptors. They can be classified into three groups comprising eight subtypes, based on sequence homology, intracellular transduction pathways, and pharmacological properties [1, 2]. The mGluR subtype 1 (mGluR1) categorized in group I is coupled with Gq proteins and can stimulate polyphosphoinositide hydrolysis, resulting in the formation of the second messengers inositol 1, 4, 5-triphosphate and diacylglycerol. Subsequently, these messengers trigger intracellular calcium release and activation of protein kinase C [3–5].

Based on these biological properties, several antagonists for mGluR1 have been developed for pharmacological studies of CNS disorders [6–10]. Additionally, several radioactive probes for mGluR1 for use in positron emission tomography (PET) have been developed to investigate mGluR1 function [11–15]. For example, the recently developed N-[4-[6-(isopropylamino)pyrimidin-4-yl]-1,3-thiazol-2-yl]-4-[^{11}C]-methoxy-N-methyl-benzamide ([^{11}C]ITMM) has initially been used for PET studies in animals and has exhibited high affinity (Ki = 12.6 nM) for mGluR1 [16]. [^{11}C]ITMM is derived from 4-fluoro-N-[4-[6-(isopropylamino)pyrimidin-4-yl]-1,3-thiazol-2-yl]-N-methylbenzamide (FITM), a potent negative allosteric modulator of mGluR1 [10]. Subsequently, [^{11}C]ITMM has been translated to first-in-human PET studies [17, 18]. In PET study of human brain, the total distribution volume (V_T) of [^{11}C]ITMM was reported as 2.61 mL/cm^3 for the cerebellum (mGluR1-rich region) and 0.52 mL/cm^3 for the pons (mGluR1-negligible region). The ranked order of corresponding V_T of [^{11}C]ITMM was cerebellum > thalamus > frontal cortex > striatum ≈ pons [18]. This distribution pattern was consistent with the known biological distribution of mGluR1 in primate brains [13].

To our knowledge, [^{11}C]ITMM is the only PET probe used to visualize mGluR1 that has been implemented in human clinical studies. Recently, several selective modulators have been used in clinical studies. The pharmacological properties of these drugs may indicate their use as treatments for psychiatric illnesses in which there is dysfunction of neuronal networks of the basal ganglia, such as in anxiety, depression, and schizophrenia [19]. PET imaging of mGluR1 in the basal ganglia is helpful for elucidating interactions between the expression of mGluR1 and disorders of these neuronal networks. However, radioactive uptake of [^{11}C]ITMM in the human striatum is low, even though mGluR1 is present throughout the mammalian brain, including the basal ganglia [2]. Therefore, to apply findings from PET (including imaging, quantification and drug occupancy assessments) to the study of these disorders, the threshold of specific binding of [^{11}C]ITMM for mGluR1 in the basal ganglia should be expanded as possible. The specific binding of radioprobe can be increased in two ways:

1. development of a radioprobe with higher binding affinity for the target molecule;

2. reduction of contamination by the nonradioactive carrier using radioprobe with high SA.

In the current study, we performed PET imaging using [^{11}C]ITMM with ultra-high SA (3,515–9,620 GBq/µmol) to improve visualization and specific binding for mGluR1.

Materials and Methods

General

All experiments were approved by the committee of the National Institute of Radiological Sciences. All chemicals and solvents used in this study were of analytic or high-performance liquid chromatography (HPLC) grade and purchased from Sigma-Aldrich (St. Louis, MO, USA), Wako Pure Industries (Osaka, Japan), and Tokyo Chemical Industries (Tokyo, Japan).

Male Sprague-Dawley (SD) rats were purchased from Japan SLC (Shizuoka, Japan), kept under the temperature-controlled environment with a 12-h light-dark cycle, and fed a standard diet (MB-1; Funabashi Farm, Chiba, Japan).
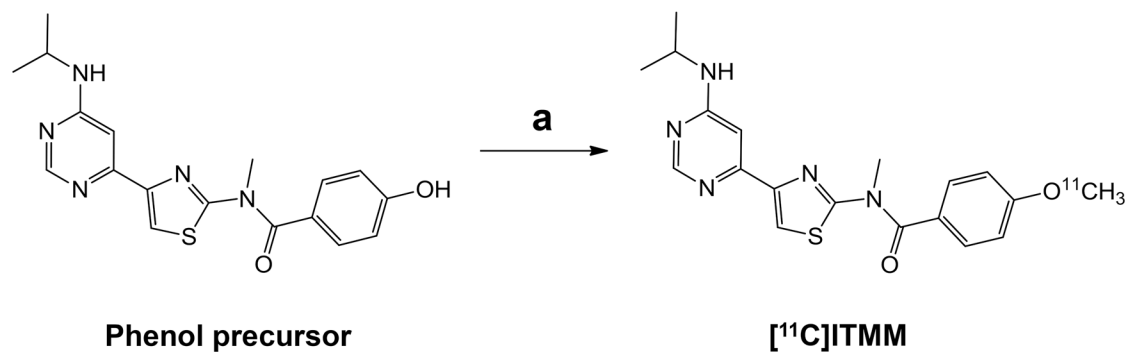
Fig 1. Radiosynthesis of [11C]ITMM with conventional or ultra-high SA.

Ethics statement

The rats were treated and handled according to the Recommendations for Handling of Laboratory Animals for Biomedical Research, compiled by the Committee on the Safety and Ethical Handling Regulations for Laboratory Animal Experiments, National Institute of Radiological Sciences, and this study was approved by the committee.

Radiochemistry

[11C]ITMM, with either conventional or ultra-high SA, was synthesized as described previously [16]. Briefly, for the conventional SA, [11C]CH$_3$I was prepared from cyclotron-produced [11C]CO$_2$ [20]. For the ultra-high SA, [11C]CH$_3$I was produced by iodination of [11C]CH$_4$ formed in the target chamber in situ (the single pass I$_2$ method) [21]. [11C]ITMM with conventional or ultra-high SA was obtained by reacting the phenol precursor with [11C]CH$_3$I in N,N-dimethylformamide (DMF) at 70°C for 5 min (Fig 1).

For the current study, [11C]ITMM with conventional SA was synthesized with 27 ± 5% radiochemical yield (decay-corrected). Starting from 14–20 GBq of [11C]CO$_2$, 1.4–2.8 GBq of [11C]ITMM was produced 27 ± 3 min after the end of bombardment (EOB). The radiochemical purity was higher than 99% and 121 ± 17 GBq/μmol (range: 74–174 GBq/μmol) of SA was obtained at the end of synthesis (EOS). [11C]ITMM with ultra-high SA was synthesized with 6 ± 1% radiochemical yield (decay-corrected). Starting from approximately 37 GBq of [11C]CH$_4$, 0.7–1.5 GBq of [11C]ITMM was produced within 32 min from EOB. The radiochemical purity was higher than 99% and 5,794 ± 1,022 GBq/μmol (range: 3,515–9,620 GBq/μmol) of SA was obtained at the EOS.

PET procedure with blood sampling

Prior to PET assessment, a SD rat had a polyethylene catheter (FR2, Imamura, Tokyo, Japan) inserted into the left femoral artery for blood sampling. Subsequently, a SD rat was secured in a custom-designed chamber and placed in a small-animal PET scanner (Inveon, Siemens Medical Solutions, Knoxville, TN, USA). Body temperature was maintained using a 40°C water circulation system (T/Pump TP401, Gaymar Industries, Orchard Park, NY, USA). A 24-gauge intravenous catheter (Terumo Medical Products, Tokyo, Japan) was placed in the tail vein of the rat for a bolus injection.

A bolus (0.5 mL) of [11C]ITMM with conventional or ultra-high SA was injected for 10 s via a catheter inserted in the tail vein. Dynamic emission scans in three-dimensional list mode were performed for 90 min (10 s x 12 frames, 20 s x 3 frames, 30 s x 3 frames, 60 s x 3 frames,

150 s x 3 frames, and 300 s x 15 frames). For counting radioactivity, blood samples were manually acquired at intervals of 10 s (0.05 mL for 50 s), 1-min intervals (0.05 mL for 5 min), and then at 10 (0.05 mL), 15 (0.2 mL), 30 (0.3 mL), 60 (0.4 mL), and 90 min (0.5 mL) after the PET scan started. For metabolite analysis, six samples of blood were obtained at 1 (0.02 mL), 5 (0.02 mL), 15 (0.05 mL), 30 (0.1 mL), 60 (0.2 mL), and 90 min (0.3 mL) after the injection. Blood samples were centrifuged at 13,000g at 4°C to separate the plasma. Levels of radioactivity in the whole blood and plasma were counted using a 1480 Wizard auto-gamma scintillation counter (Perkin-Elmer, Waltham, MA, USA). The radioactivity was corrected for decay.

Metabolite analysis was performed as described previously [22]. Briefly, whole blood samples were treated to separate the plasma, which was deproteinized with an equivalent amount of acetonitrile. An aliquot of the supernatant obtained from the plasma was analyzed by HPLC with a radiation detector [23]. Plasma protein binding was not determined in the present study. The time curves for the fraction of unchanged [^{11}C]ITMM in the plasma were fitted using three exponential equations, and subsequently used for kinetic analysis.

PET dynamic images were reconstructed with filtered back projection using a Hunning filter with a Nyquist cut-off of 0.5 cycle/pixel. PET/MRI fused images were acquired by PMOD version 3.4 (PMOD Technologies, Zurich, Switzerland). To generate the time-activity curves (TACs) of specified brain regions, volumes of interest (VOIs) were drawn encompassing the cerebellum, hippocampus, thalamus, striatum, cingulate cortex, substantia nigra, and pons. The radioactivity was decay-corrected to the injection time and is expressed as the standardized uptake value (SUV), which was normalized to the injected radioactivity and body weight [24]. SUV was calculated according to the following formula: SUV = (radioactivity per milliliter tissue / injected radioactivity) × gram body weight.

Estimation of equilibrium state

Estimations of the equilibrium state of [^{11}C]ITMM in each brain region were obtained using averaged plasma input functions and averaged tissue TACs. Theoretical radioactive concentrations in each brain region (C_t') and the plasma input function of [^{11}C]ITMM (C_P') were estimated using averaged measurements extracted between 5 and 90 min after the injection and subjected to three exponential least square fitting [Radioactivity (t) = A*exp(-at) + B*exp(-bt) + C*exp(-ct)].

The estimations over 90 min after the injection were calculated by extrapolating based on the equation as described above. The time at which equilibrium state was reached in each brain region was determined by the peak of the time-course of tissue-to-plasma concentration ratios, C_t'(t)/C_P'(t).

To confirm validity of PET scanning time in this study, scatter plot analysis of measured and estimated values was performed using V_T values based on Logan graphical analysis (GA) [25].

Two-tissue compartment model analysis

Kinetic analysis of [^{11}C]ITMM was performed using the two-tissue compartment model (2TCM) [26, 27]. The compartments correspond to the radioactivity concentrations of unchanged radioprobe in the plasma (C_P), free and non-specifically bound radioprobe (C_1), and radioprobe specifically bound to receptors (C_2). The rate constants K_1 and k_2 correspond to the influx and outflux rates of the radioprobe across the blood-brain barrier. The rate constants k_3 and k_4 correspond to the rates of radioprobe transfer between the C_1 and C_2 compartments. The blood volume fraction (vB) in the rat brain was fixed at 2% [28]. The four rate constants of the 2TCM were obtained by a nonlinear least squares fitting technique, using PMOD version 3.4 (PMOD Technologies).

The distribution of [¹¹C]ITMM in free or tissue compartments was described using the concept of free ligand distribution volume (DV_f) or V_T, which was defined by the following equations:

$$DV_f = \frac{K_1}{k_2} \tag{1}$$

$$V_T = DV_f \left(1 + \frac{k_3}{k_4} \right) \tag{2}$$

The nondisplacable binding potential (BP_{ND}) is defined using the index of specific bindings of the radioprobe, meaning the receptor density (B_{max}) to binding affinity (K_D) ratio, which corresponds with the ratio of k_3 to k_4 in the 2TCM [26]. The BP_{ND} is defined as follows:

$$BP_{ND} = f_{ND} \cdot \frac{B_{\max}}{K_D} = \frac{k_3}{k_4} \tag{3}$$

Here, f_{ND} represents the tissue-free fraction of radioprobe in the nondisplacable compartment [29]. Although the fraction of radioprobe that is unbound to plasma proteins was not measured in the present study, the value of f_{ND} is close to 1.0 [29].

Parametric images

The ratio of vascular radioactivity contribution was fixed at 2%, and eliminated prior to the parameter estimation. Parameter estimates were considered outliers if V_T value was outside the range $0 < V_T < 25$. The parametric image was acquired in PMOD version 3.4 (PMOD Technologies).

Statistics

Kinetic model selection was determined using three statistical methods: the Akaike information criterion [30]; the Schwarz criterion [31]; and the Model Selection criterion.

The standard error (s.e.) of the parameter was given by the diagonal of the covariance matrix, expressed as a percentage of the parameter value (coefficient of variation, %COV) and used to validate the parameter by a nonlinear least square fitting procedure [32].

All data are expressed as the mean ± s.e. Differences between the two SAs were calculated using a two-way ANOVA. Significance was determined at $p < 0.05$. The data were analyzed by GraphPad Prism 5 software (GraphPad Software, San Diego, CA, USA).

Results

Small-animal PET study

[¹¹C]ITMM with ultra-high SA of 3,515–9,620 GBq/µmol contained 10.9 ± 1.6 pmol of nonradioactive carrier in the injected solution. Meanwhile, [¹¹C]ITMM conventional SA of 74–174 GBq/µmol included 513.1 ± 58.7 pmol of nonradioactive carrier in the injected solution (Table 1).

Fig 2 shows TACs of [¹¹C]ITMM with conventional (A) or ultra-high (B) SA in the cerebellum, thalamus, hippocampus, striatum, cingulate cortex, substantia nigra, and pons. The maximum uptake of [¹¹C]ITMM with the conventional SA was 3.0 in the cerebellum, 2.3 in the thalamus, 2.0 in the hippocampus, 2.1 in the striatum, 2.0 in the cingulate cortex, 1.8 in the substantia nigra, and 0.9 SUV in the pons. Meanwhile, the maximum uptake of [¹¹C]ITMM with ultra-high SA was 3.4 in the cerebellum, 2.6 in the thalamus, 2.2 in the hippocampus, 2.4

Table 1. Characteristics of animals used and experimental data from the two conditions using [^{11}C]ITMM with conventional or ultra-high SA in PET (means ± s.e.).

	Conventional SA	Ultra-high SA
Age (weeks old)	7–9	8
Gender	male	male
Body weight (g)	280.9 ± 10.1	281.2 ± 6.7
Subjects	5	5
Radioactivity (MBq)/head	57.7 ± 1.2	56.6 ± 1.4
Carrier dose (pmol)/head	513.1 ± 58.7	10.9 ± 1.6

doi:10.1371/journal.pone.0130006.t001

in the striatum, 2.3 in the cingulate cortex, 2.2 in the substantia nigra, and 0.9 SUV in the pons. Moreover, the peak time of radioactivity with the ultra-high SA was delayed by 4–10 min compared with the conventional SA.

Estimation of equilibrium state

The metabolite corrected input functions after intravenous injection of [^{11}C]ITMM with conventional and ultra-high SA are shown in Fig 3. Radioactivity appeared rapidly, initially (< 1 min) at high levels in the plasma, and then it quickly decreased. The radioactivity in the plasma was roughly 55% of unchanged [^{11}C]ITMM at 15 min, decreasing to roughly 15% 90 min after the injection of the two SAs (Table 2).

Fig 4 shows time-courses of estimated tissue-to-plasma concentration ratios, C_t'(t)/C_P'(t), for [^{11}C]ITMM with conventional or ultra-high SA in the (A) cerebellum, (B) thalamus, (C) hippocampus, (D) striatum, (E) cingulate cortex, (F) substantia nigra, and (G) pons. The estimated equilibrium times (min) of [^{11}C]ITMM with conventional and ultra-high SA were 150 and 150 for the cerebellum, 120 and 140 for the thalamus, 120 and 130 for the hippocampus, 120 and 130 for the striatum, 100 and 120 for the cingulate cortex, 110 and 100 for the substantia nigra, and 110 and 100 for the pons, respectively. In this study, PET assessments with blood sampling were performed for 90 min because of the short half-life of ^{11}C. Uptake of
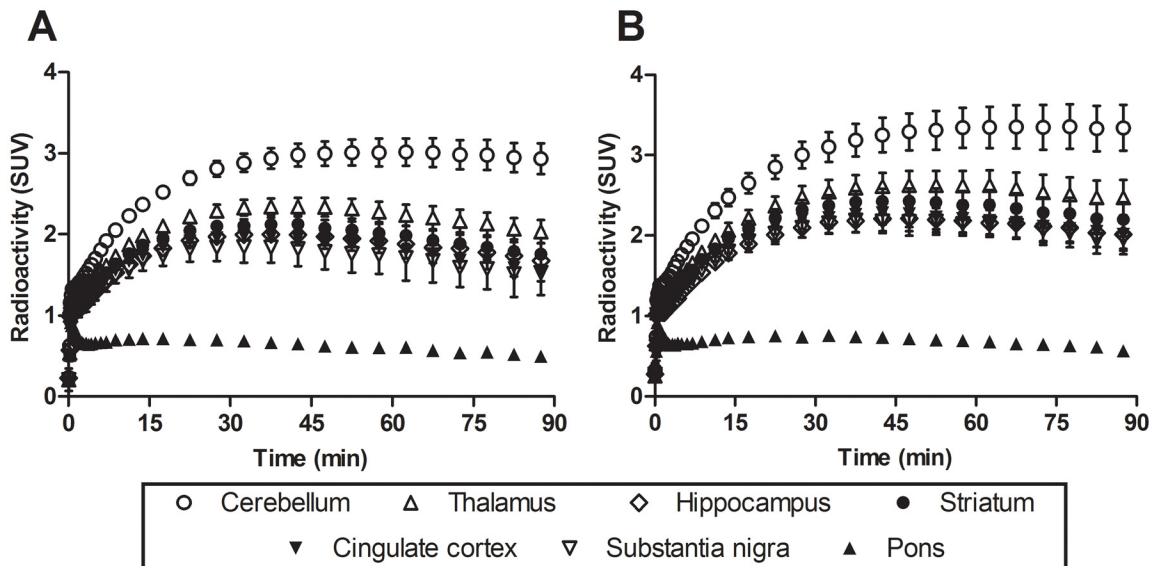

Fig 2. Time-activity curves of [^{11}C]ITMM with (A) conventional SA and (B) ultra-high SA.
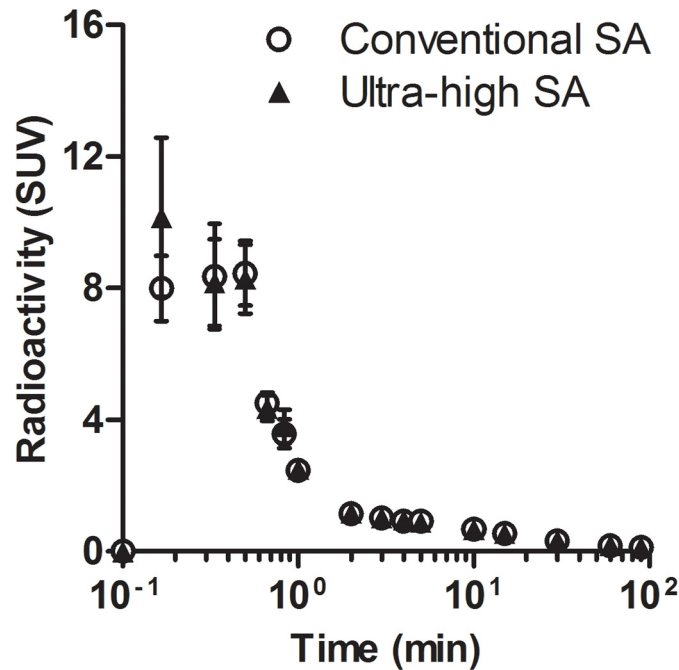
doi:10.1371/journal.pone.0130006.g002

Fig 3. The metabolite-corrected input function of [¹¹C]ITMM with conventional or ultra-high SA in the plasma.

radioactivity of [¹¹C]ITMM with conventional and ultra-high SA in the brain regions reached 80 and 82 of equilibrium state in the cerebellum, 91 and 87 in the thalamus, 93 and 89 in the hippocampus, 93 and 90 in the striatum, 96 and 91 in the cingulate cortex, 94 and 98 in the substantia nigra, and 94 and 98% in the pons, respectively.

Fig 4H shows correlations between measured- and estimated-V_T values based on Logan GA. A high correlation was seen between the measured and estimated values.

Two-tissue compartment model analysis

Details of full kinetic parameters using 2TCM with metabolite-corrected plasma input functions are given in Table 3 for conventional SA and in Table 4 for ultra-high SA. The rate constants (K_1–k_4) in both experimental groups were acquired with relatively low %COV. The range of %COV for constant K_1 in conventional and ultra-high SA experiments was 3.5–9.9

Table 2. Percentage of unchanged [¹¹C]ITMM with conventional or ultra-high SA in the plasma (means ± s.e., n = 5 in each group).

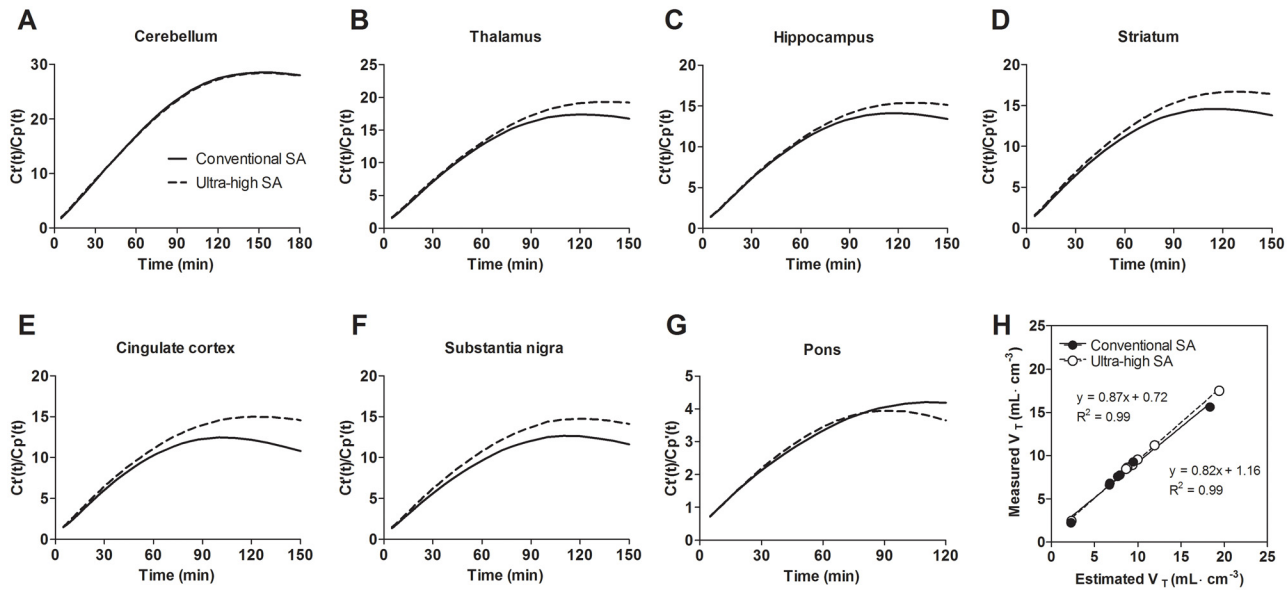| Time after injection (min)	Unchanged form (%)	
	Conventional SA	Ultra-high SA
1	95.2 ± 1.2	97.3 ± 0.6
5	74.0 ± 2.1	77.1 ± 3.2
15	53.7 ± 2.6	56.2 ± 4.0
30	36.8 ± 2.6	40.0 ± 4.0
60	21.7 ± 2.0	24.7 ± 2.9
90	15.7 ± 1.3	18.2 ± 2.5

Fig 4. Estimated tissue-to-plasma concentration ratio, $C_t'(t)/C_P'(t)$, of [^{11}C]ITMM with conventional or ultra-high SA and scatter plots indicating the relationship between measured- and estimated-V_T values.

doi:10.1371/journal.pone.0130006.g004

Table 3. Full kinetic parameters of [^{11}C]ITMM with conventional SA using 2TCM.

	Region	K_1 (mL/cm^3/min)	k_2 (/min)	k_3 (/min)	k_4 (/min)	V_T (mL/cm^3)	DV_f (K_1/k_2)	BP_{ND} (k_3/k_4)	AUC (SUV · min)
Mean ± s. e. (n = 5)									
	Cerebellum	0.344 ± 0.010	0.811 ± 0.045	0.619 ± 0.035	0.019 ± 0.001	14.56 ± 0.50	0.429 ± 0.020	33.2 ± 1.4	243.2 ± 9.2
	Thalamus	0.303 ± 0.012	0.886 ± 0.064	0.669 ± 0.033	0.026 ± 0.001	9.12 ± 0.37	0.347 ± 0.018	25.5 ± 1.2	188.4 ± 6.9
	Hippocampus	0.303 ± 0.015	1.052 ± 0.082	0.644 ± 0.051	0.026 ± 0.001	7.44 ± 0.27	0.292 ± 0.011	24.8 ± 1.8	160.8 ± 4.6
	Striatum	0.278 ± 0.014	0.769 ± 0.061	0.612 ± 0.036	0.031 ± 0.001	7.66 ± 0.28	0.367 ± 0.015	20.0 ± 1.1	169.7 ± 6.0
	Cingulate cortex	0.312 ± 0.008	1.062 ± 0.086	0.643 ± 0.053	0.030 ± 0.001	6.76 ± 0.25	0.302 ± 0.021	21.7 ± 1.2	156.9 ± 5.3
	Substantia nigra	0.298 ± 0.021	0.840 ± 0.128	0.470 ± 0.031	0.029 ± 0.001	6.44 ± 0.22	0.378 ± 0.030	16.6 ± 1.6	149.9 ± 6.7
	Pons	0.271 ± 0.015	1.237 ± 0.122	0.256 ± 0.022	0.031 ± 0.001	2.06 ± 0.06	0.224 ± 0.011	8.3 ± 0.5	56.0 ± 1.6
%COV									
	Cerebellum	5.90 ± 0.51	17.73 ± 0.89	10.56 ± 0.53	5.95 ± 0.34	2.53 ± 0.25	12.38 ± 0.53	12.3 ± 0.5	-
	Thalamus	5.46 ± 0.56	16.27 ± 1.16	9.79 ± 0.78	4.99 ± 0.37	1.65 ± 0.19	11.32 ± 0.79	11.5 ± 0.8	-
	Hippocampus	6.15 ± 0.41	16.30 ± 1.02	9.76 ± 0.78	5.05 ± 0.36	1.86 ± 0.17	10.78 ± 0.79	10.9 ± 0.8	-
	Striatum	5.23 ± 0.48	16.69 ± 1.50	10.69 ± 1.14	5.12 ± 0.48	1.58 ± 0.18	11.95 ± 1.22	12.3 ± 1.3	-
	Cingulate cortex	6.97 ± 0.72	18.28 ± 1.74	10.94 ± 0.82	5.52 ± 0.39	1.88 ± 0.10	12.01 ± 1.14	12.3 ± 1.2	-
	Substantia nigra	5.87 ± 0.41	15.36 ± 0.87	10.18 ± 1.23	5.37 ± 0.43	2.06 ± 0.18	10.10 ± 1.12	10.5 ± 1.2	-
	Pons	7.72 ± 1.07	13.32 ± 1.24	11.38 ± 0.86	8.95 ± 0.69	4.01 ± 0.29	6.83 ± 0.47	8.0 ± 0.6	-

V_T: total distribution volume; DV_f: distribution volume of free ligand; BP_{ND}: nondisplacable binding potential; AUC: area under the curve.

doi:10.1371/journal.pone.0130006.t003

Table 4. Full kinetic parameters of [11C]ITMM with ultra-high SA using 2TCM.

	Region	K_1 (mL/cm³/min)	k_2 (/min)	k_3 (/min)	k_4 (/min)	V_T (mL/cm³)	DV_f (K_1/k_2)	BP_{ND} (k_3/k_4)	AUC (SUV · min)
Mean ± s.e. (n = 5)									
	Cerebellum	0.366 ± 0.019	1.112 ± 0.098	0.799 ± 0.035	0.016 ± 0.000	16.69 ± 0.92	0.336 ± 0.020	48.9 ± 2.6	269.9 ± 15.8
	Thalamus	0.313 ± 0.016	1.125 ± 0.088	0.817 ± 0.025	0.021 ± 0.000	11.15 ± 0.51	0.284 ± 0.018	38.5 ± 1.1	214.2 ± 12.2
	Hippocampus	0.320 ± 0.020	1.415 ± 0.107	0.784 ± 0.027	0.021 ± 0.000	8.93 ± 0.47	0.228 ± 0.008	38.2 ± 1.5	180.2 ± 10.9
	Striatum	0.294 ± 0.014	0.972 ± 0.083	0.722 ± 0.043	0.024 ± 0.001	9.66 ± 0.41	0.311 ± 0.021	30.6 ± 1.8	197.3 ± 11.1
	Cingulate cortex	0.339 ± 0.019	1.317 ± 0.054	0.740 ± 0.036	0.023 ± 0.001	8.66 ± 0.45	0.257 ± 0.008	32.8 ± 1.9	184.7 ± 11.1
	Substantia nigra	0.292 ± 0.012	0.933 ± 0.075	0.602 ± 0.036	0.023 ± 0.001	8.53 ± 0.47	0.321 ± 0.023	26.1 ± 2.0	178.9 ± 10.8
	Pons	0.244 ± 0.004	1.131 ± 0.084	0.253 ± 0.011	0.026 ± 0.001	2.39 ± 0.23	0.221 ± 0.015	9.8 ± 0.5	62.7 ± 3.6
%COV									
	Cerebellum	4.38 ± 0.84	10.51 ± 2.64	6.54 ± 0.76	4.64 ± 0.22	1.99 ± 0.15	7.31 ± 1.46	7.5 ± 1.3	-
	Thalamus	5.27 ± 0.90	14.76 ± 1.91	8.07 ± 0.92	4.45 ± 0.52	1.52 ± 0.18	9.96 ± 1.13	9.9 ± 1.1	-
	Hippocampus	5.68 ± 0.80	13.46 ± 1.46	7.13 ± 0.69	3.98 ± 0.39	1.61 ± 0.17	8.34 ± 0.77	8.3 ± 0.8	-
	Striatum	4.55 ± 0.67	13.17 ± 1.68	7.60 ± 0.95	4.02 ± 0.50	1.39 ± 0.20	9.03 ± 1.09	9.1 ± 1.1	-
	Cingulate cortex	6.42 ± 0.56	15.82 ± 1.48	8.78 ± 0.84	4.77 ± 0.45	1.86 ± 0.16	10.05 ± 1.02	10.0 ± 1.0	-
	Substantia nigra	5.34 ± 0.46	14.62 ± 1.00	8.90 ± 0.67	4.73 ± 0.35	1.90 ± 0.17	9.82 ± 0.63	9.9 ± 0.6	-
	Pons	6.15 ± 0.54	11.45 ± 0.70	10.05 ± 0.63	8.22 ± 0.60	3.84 ± 0.25	6.39 ± 0.29	7.2 ± 0.3	-

doi:10.1371/journal.pone.0130006.t004

and 2.1–9.1, respectively. For constant k_2, it was 9.6–25.3 and 8.9–22.9. For constant k_3, it was 6.5–14.4 and 4.3–12.6. For constant k_4, it was 3.4–11.6 and 3.0–10.2.

A comparison of kinetic parameters between the two SAs is shown in Fig 5. There were no differences in K_1 between the two SAs in any brain regions. Meanwhile, k_2 in the ultra-high SA tended to be higher compared with the conventional SA, except in the pons. Moreover, k_3 in the ultra-high SA was higher in all brain regions except the pons compared with the conventional SA. In contrast, k_4 of the thalamus, hippocampus, striatum, cingulate cortex, substantia nigra, and pons in the ultra-high SA condition was significantly lower compared with the conventional SA. Correspondingly, the V_T, area under the curve (AUC) and BP_{ND} in the ultra-high SA condition were higher than in the conventional SA. In particular, significant differences (p < 0.001) were observed in the BP_{ND} of the two SAs in the cerebellum, thalamus, hippocampus, striatum, cingulate cortex, and substantia nigra. Conversely, the DV_f of each brain region in the ultra-high SA condition tended to be lower compared with the conventional SA condition.

Parametric PET imaging

Fig 6 shows representative parametric PET/MRI fused images scaled according to V_T. The signals for [11C]ITMM with ultra-high SA were noticeably higher than with the conventional SA in the cingulate cortex, striatum, thalamus, hippocampus, substantia nigra, and cerebellum. In particular, signals of the cingulate cortex and substantia nigra in the ultra-high SA were more identifiable than that in the conventional SA.

Discussion

In the present study, we demonstrated that the specific binding of [11C]ITMM with ultra-high SA for mGluR1 was significantly increased in several brain regions compared with that of [11C]
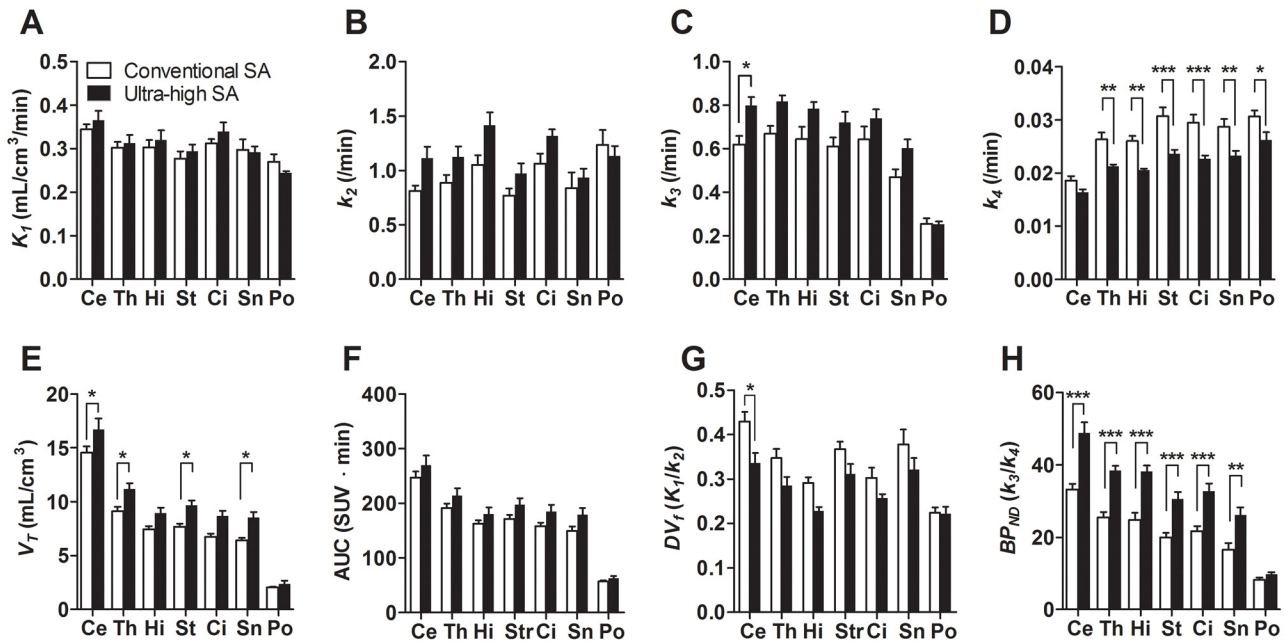
Fig 5. Differences in kinetic parameters between [11C]ITMM with conventional and ultra-high SA.
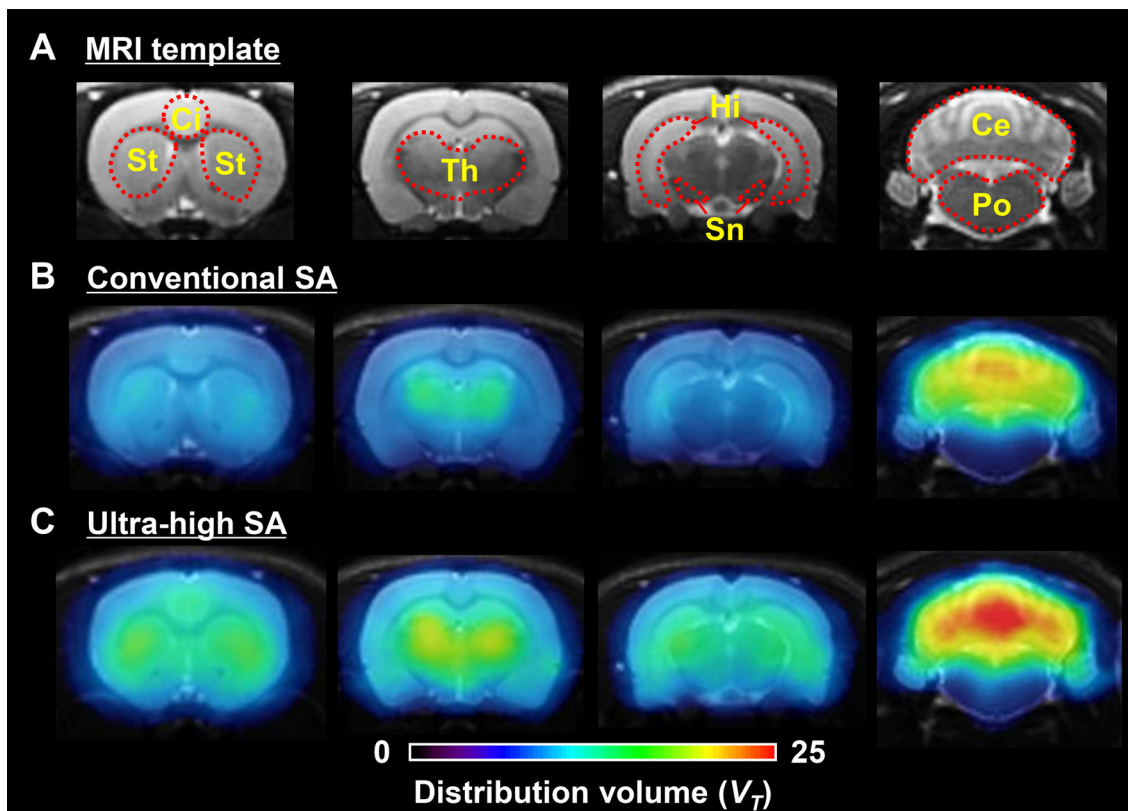
Fig 6. Representative parametric PET/MRI fused images based on V_T scale.

ITMM with conventional SA. In addition, V_T-scaled parametric PET images of [11C]ITMM with ultra-high SA allowed more accurate identification of regional differences in mGluR1 than with the conventional SA.

Several [11C]radioprobes have been developed with ultra-high SA to increase specific binding and to visualize target molecules with low density [21, 33–37]. In the case of [11C]DAC, a selective PET probe for a translocater protein (TSPO) known to be a biomarker of inflammation, ultra-high SA has been demonstrated to exhibit a binding potential on the ipsilateral side of an ischemic rat brain roughly two times higher than with the conventional SA [36]. Thus, use of radioprobes with ultra-high SA has the potential to improve visualization and threshold of specific binding for target molecules with low density.

[11C]ITMM with ultra-high SA has been successfully synthesized as reported previously, but is yet to be evaluated as its application has not been investigated [16]. Here, the comparison between [11C]ITMM with conventional and ultra-high SA was performed using kinetic analysis by 2TCM.

Averaged PET images of [11C]ITMM with ultra-high SA showed a slight improvement compared with the conventional SA (S1 Fig). Additionally, its TAC indicated increased radioactive uptake in several brain regions (Fig 2). However, the ratio of tissue-to-plasma concentrations of [11C]ITMM did not reach equilibrium in either SA condition during the 90-min acquisition. Prior to kinetic analysis with 2TCM, we estimated equilibrium states by simulating estimated plasma input functions and tissue TACs (S2 and S3 Figs). The equilibrium times in both SA conditions were determined within 100–150 min after the injection (Fig 4A–4G). Unfortunately, PET with [11C]ITMM was impossible to perform under the equilibrium state, because radioactivity of plasma input function 90 min after the injection was very low. More importantly, [11C]ITMM bindings reached 80–98% of the equilibrium state, and there was high correlation between measured and estimated V_T values in both SA conditions (Fig 4H). These results permit kinetic analysis with 2TCM using tissue TACs acquired from PET scans of 90 min.

The results of the kinetic analysis with 2TCM (Fig 5) indicated small differences between the two SA values for constants K_1 and k_2, but relatively large differences for the constants k_3 and k_4. In particular, a significant difference in BP_{ND} (k_3/k_4) was observed between the two SAs in the cerebellum, thalamus, hippocampus, striatum, cingulate cortex and substantia nigra. Similarly, V_T values in the cerebellum, thalamus, striatum and substantia nigra were detected with significant differences between the two SAs. These results demonstrate remarkable differences in the specific binding for mGluR1 between the two SA values.

When [11C]ITMM with conventional SA containing 355–732 pmol of nonradioactive carrier was administered, about 4–7 pmol/mL of nonradioactive carrier was estimated to reach the brain. Meanwhile, contamination by nonradioactive carrier in the administration of [11C] ITMM with ultra-high SA would be negligible (6–17 pmol). Previously, densities (B_{max}) of mGluR1 in the rat brain have been reported as follows: 36 in the thalamus, 28 in the hippocampus, 22 in the striatum, and 20 pmol/mL in the cingulate cortex [27]. It can be assumed that 10–20% of specific binding in PET images using [11C]ITMM with conventional SA was occupied by nonradioactive carrier. Increases in the BP_{ND} and specific binding for mGluR1 of [11C] ITMM with ultra-high SA were due to a reduction in the level of nonradioactive carrier. However, in the cerebellum, the mGluR1-richest region, significant increment of specific binding of [11C]ITMM with ultra-high SA was detected. In our previous unpublished data, in vitro binding assay with [18F]FITM, an analogue of [11C]ITMM, using cerebellum homogenate has exhibited two binding sites of [18F]FITM possessing high and low affinities (S4 Fig). Hence, increments of binding of [11C]ITMM with ultra-high SA in the cerebellum would be caused by decrease of carrier exposure in a binding site with low affinity.

The V_T-scaled parametric PET images of [11C]ITMM with ultra-high SA significantly improved visualization of mGluR1 in mGluR1-moderate or-low regions compared with the conventional SA (Fig 6). These images showed a significant improvement in the specific binding for mGluR1 using [11C]ITMM with ultra-high SA.

We found significant differences between the two SAs in the basal ganglia, such as striatum, thalamus, and substantia nigra. In previous studies, the B_{max} of mGluR1 in the human cerebral cortex was 26 pmol/mL, but has not been reported for the striatum [11]. The radioactive uptake (SUV) of [11C]ITMM with conventional SA in the human striatum is half that of the cerebral cortex [18]. This result suggests that the B_{max} in human striatum would at most be less than half of 26 pmol/mL. In a first-in human PET study using [11C]ITMM, 0.001–0.004% of the injection dose/mL of [11C]ITMM containing 5.5–12 nmol nonradioactive carrier reached the brains of healthy humans [18] This suggests that 0.1–0.5 pmol/mL nonradioactive carrier would occupy the binding sites of mGluR1 in human brains, which is lower by one order than rodents. Although the influence on receptor occupancy by nonradioactive carrier in human subjects is small, radioactive uptake in very low-density regions would be affected. In fact, radiolabeling techniques with ultra-high SA has enabled observation of slight differences in regions with very low density of the target receptor (0.7–2.3 pmol/mL for extrastriatal dopamine D_2 receptors) [33]. Hence, PET studies using [11C]ITMM with ultra-high SA may permit detection of significant regional differences in mGluR1 in the basal ganglia of humans.

Interestingly, mGluR1 pathology in neurodegenerative disorders is beginning to be understood using experimental models in rodents and nonhuman primates. In a mouse model of Huntington's disease, in which there is reduced binding of [3H]dopamine in the striatum, a significant decrease in mGluR1 but not mGluR5 was detected in the basal ganglia [38]. Furthermore, decreased striatal mGluR1 was reported in a rat model of ischemic stroke [39]. In nonhuman primates, mGluR1 expression is decreased in the globus pallidus and substantia nigra in Parkinson's disease [40]. Although clinical studies in humans are very important, investigating mGluR1 in experimental animal models can help further understanding of the interactions between dysfunction of mGluR1 and related pathologies. Therefore, improving the specific binding of [11C]ITMM with ultra-high SA for mGluR1 will improve visualization in the rat brain, allowing clear detection of early mGluR1 changes in experimental models of brain diseases.

Conclusions

[11C]ITMM with ultra-high SA demonstrated improved specific binding for mGluR1 in several brain regions, particularly in the thalamus, striatum, and substantia nigra. In vivo monitoring of mGluR1 by PET using [11C]ITMM with ultra-high SA can further our understanding of unknown mechanisms of mGluR1, and may help in the development of new medications for CNS disorders, such as schizophrenia.

Supporting Information

S1 Fig. Representative PET/MRI fused images of [11C]ITMM with (A) conventional SA and (B) ultra-high SA in the cingulate cortex (Ci)/striatum (Str), hippocampus (Hi)/thalamus (Th), and cerebellum (Ce)/pons (Po) coronal slices. The colored scale bar represents levels of radioactive uptake (standardized uptake value, SUV).
(TIF)

S2 Fig. Theoretical plasma input Cp) and tissue time-activity (Ct) curves of [11C]ITMM with conventional SA in the cerebellum (A), thalamus (B), hippocampus (C), striatum (D),

cingulate cortex (E), substantia nigra (F), and pons (G). Non-linear regressions were performed with three-term exponential curve fitting.
(TIF)

S3 Fig. Theoretical plasma input (Cp) and tissue time-activity (Ct) curves of [^{11}C]ITMM with ultra-high SA in the cerebellum (A), thalamus (B), hippocampus (C), striatum (D), cingulate cortex (E), substantia nigra (F), and pons (G). Non-linear regressions were performed by three-term exponential curve fitting.
(TIF)

S4 Fig. Scatter plots analysis on in vitro binding assay with [^{18}F]FITM using cerebellum homogenate.
(TIF)

Acknowledgments

Author Contributions

Conceived and designed the experiments: TY MRZ. Performed the experiments: TY JY AH LX. Analyzed the data: TY HW TO YI KK. Contributed reagents/materials/analysis tools: MF NN MO. Wrote the paper: TY MRZ.

References

1. Hermans E, Challiss RA. Structural, signalling and regulatory properties of the group I metabotropic glutamate receptors: prototypic family C G-protein-coupled receptors. Biochem J. 2001; 359: 465–484. PMID: 11672421

2. Ferraguti F, Crepaldi L, Nicoletti F. Metabotropic glutamate 1 receptor: current concepts and perspectives. Pharmacol Rev. 2008; 60: 536–581. doi: 10.1124/pr.108.000166 PMID: 19112153

3. Aramori I, Nakanishi S. Signal transduction and pharmacological characteristics of a metabotropic glutamate receptor, mGluR1, in transfected CHO cells. Neuron. 1992; 8: 757–765. PMID: 1314623

4. Francesconi A, Duvoisin RM. Role of the second and third intracellular loops of metabotropic glutamate receptors in mediating dual signal transduction activation. J Biol Chem. 1998; 273: 5615–5624. PMID: 9488690

5. Di Matteo V, De Blasi A, Di Giulio C, Esposito E. Role of 5-HT2C receptors in the control of central dopamine function. Trends Pharmacol Sci. 2001; 22: 229–232. PMID: 11339973

6. Hermans E, Nahorski SR, Challiss RA. Reversible and non-competitive antagonist profile of CPCCOEt at the human type 1alpha metabotropic glutamate receptor. Neuropharmacology. 1998; 37: 1645–1647. PMID: 9886688

7. De Vry J, Horvath E, Schreiber R. Neuroprotective and behavioral effects of the selective metabotropic glutamate mGlu1 receptor antagonist BAY 36–7620. Eur J Pharmacol. 2001; 428: 203–214. PMID: 11675037

8. Makarewicz D, Duszczyk M, Gadamski R, Danysz W, Lazarewicz JW. Neuroprotective potential of group I metabotropic glutamate receptor antagonists in two ischemic models. Neurochem Int. 2006; 48: 485–490. PMID: 16513218

9. Kohara A, Takahashi M, Yatsugi S, Tamura S, Shitaka Y, Hayashibe S, et al. Neuroprotective effects of the selective type 1 metabotropic glutamate receptor antagonist YM-202074 in rat stroke models. Brain Res. 2008; 1191: 168–179. doi: 10.1016/j.brainres.2007.11.035 PMID: 18164695

10. Satoh A, Nagatomi Y, Hirata Y, Ito S, Suzuki G, Kimura T, et al. Discovery and in vitro and in vivo profiles of 4-fluoro-N-[4-[6-(isopropylamino)pyrimidin-4-yl]-1,3-thiazol-2-yl]-N-methy lbenzamide as novel class of an orally active metabotropic glutamate receptor 1 (mGluR1) antagonist. Bioorg Med Chem Lett. 2009; 19; 5464–5468. doi: 10.1016/j.bmcl.2009.07.097 PMID: 19674894

11. Yanamoto K, Konno F, Odawara C, Yamasaki T, Kawamura K, Hatori A, et al. Radiosynthesis and evaluation of [11C]YM-202074 as a PET ligand for imaging the metabotropic glutamate receptor type 1. Nucl Med Biol. 2010; 37: 615–624. doi: 10.1016/j.nucmedbio.2010.03.002 PMID: 20610166

12. Fujinaga M, Maeda J, Yui J, Hatori A, Yamasaki T, Kawamura K, et al. Characterization of 1-(2-[18F] fluoro-3-pyridyl)-4-(2-isopropyl-1-oxo-isoindoline-5-yl)-5-methyl-1H-1,2,3-triazole, a PET ligand for imaging the metabotropic glutamate receptor type 1 in rat and monkey brains. J Neurochem. 2012; 121: 115–124. doi: 10.1111/j.1471-4159.2011.07348.x PMID: 21668889

13. Hostetler ED, Eng W, Joshi AD, Sanabria-Bohorquez S, Kawamoto H, Ito S, et al. Synthesis, characterization, and monkey PET studies of [18F]MK-1312, a PET tracer for quantification of mGluR1 receptor occupancy by MK-5435. Synapse. 2011; 65: 125–135. doi: 10.1002/syn.20826 PMID: 20524178

14. Prabhakaran J, Majo VJ, Milak MS, Kassir SA, Palner M, Savenkova L, et al. Synthesis, in vitro and in vivo evaluation of [11C]MMTP: a potential PET ligand for mGluR1 receptors. Bioorg Med Chem Lett. 2011; 20: 3499–3501.

15. Yamasaki T, Fujinaga M, Yoshida Y, Kumata K, Yui J, Kawamura K, et al. Radiosynthesis and preliminary evaluation of 4-[18F]fluoro-N-[4-[6-(isopropylamino)pyrimidin-4-yl]-1,3-thiazol-2-yl]-N-methylbenzamide as a new positron emission tomography ligand for metabotropic glutamate receptor subtype 1. Bioorg Med Chem Lett. 2011; 21: 2998–3001. doi: 10.1016/j.bmcl.2011.03.046 PMID: 21470858

16. Fujinaga M, Yamasaki T, Yui J, Hatori A, Xie L, Kawamura K, et al. Synthesis and evaluation of novel radioligands for positron emission tomography imaging of metabotropic glutamate receptor subtype 1 (mGluR1) in rodent brain. J Med Chem. 2012; 55: 2342–2352. doi: 10.1021/jm201590g PMID: 22316010

17. Toyohara J, Sakata M, Fujinaga M, Yamasaki T, Oda K, Ishii K, et al. Preclinical and the first clinical studies on [11C]ITMM for mapping metabotropic glutamate receptor subtype 1 by positron emission tomography. Nucl Med Biol. 2013; 40: 214–220. doi: 10.1016/j.nucmedbio.2012.11.008 PMID: 23265669

18. Toyohara J, Sakata M, Oda K, Ishii K, Ito K, Hiura M, et al. Initial human PET studies of metabotropic glutamate receptor type 1 ligand 11C-ITMM. J Nucl Med. 2013; 54: 1302–1307. doi: 10.2967/jnumed. 113.119891 PMID: 23804329

19. Lesage A, Steckler T. Metabotropic glutamate mGlu1 receptor stimulation and blockade: therapeutic opportunities in psychiatric illness. Eur J Pharmacol. 2010; 639: 2–16. doi: 10.1016/j.ejphar.2009.12. 043 PMID: 20371230

20. Suzuki K, Inoue O, Hashimoto K, Yamasaki T, Kuchiki M, Tamate K. Computer-controlled large scale production of high specific activity [11C]RO15-1788 for PET studies of benzodiazepine receptors. Int J Appl Radiat Isot. 1985; 36: 971–976. PMID: 3002988

21. Noguchi J, Suzuki K, Automated synthesis of the ultra high specific activity of [11C]Ro15-4513 and its application in an extremely low concentration region to an ARG study. Nucl Med Biol. 2003; 30: 335–343. PMID: 12745025

22. Yamasaki T, Maeda J, Fujinaga M, Nagai Y, Hatori A, Yui J, et al. PET brain kinetics studies of 11C-ITMM and 11C-ITDM,radioprobes for metabotropic glutamate receptor type 1, in a nonhuman primate. Am J Nucl Med Mol Imaging. 2014; 4: 260–269. PMID: 24795840

23. Takei M, Kida T, Suzuki K. Sensitive measurement of positron emitters eluted from HPLC. Appl Radiat Isot. 2001; 55: 229–234. PMID: 11393764

24. Keyes JW Jr. SUV: standard uptake or silly useless value? J Nucl Med. 1995; 36: 1836–1839. PMID: 7562051

25. Logan J, Fowler JS, Volkow ND, Wolf AP, Dewey SL, Schlyer DJ, et al. Graphical analysis of reversible radioligand binding from time-activity measurements applied to [N-11C-methyl]-(-)-cocaine PET studies in human subjects. J Cereb Blood Flow Metab. 1990; 10: 740–747. PMID: 2384545

26. Mintun MA, Raichle ME, Kilbourn MR, Wooten GF, Welch MJ. A quantitative model for the in vivo assessment of drug binding sites with positron emission tomography. Ann Neurol. 1984; 15: 217–227. PMID: 6609679

27. Koeppe RA, Holthoff VA, Frey KA, Kilbourn MR, Kuhl DE. Compartmental analysis of [11C]flumazenil kinetics for the estimation of ligand transport rate and receptor distribution using positron emission tomography. J Cereb Blood Flow Metab. 1991; 11: 735–744. PMID: 1651944

28. Yamasaki T, Fujinaga M, Kawamura K, Yui J, Hatori A, Ohya T, et al. In vivo measurement of the affinity and density of metabotropic glutamate receptor subtype 1 in rat brain using 18F-FITM in small-animal PET. J Nucl Med. 2012; 53: 1601–1607. doi: 10.2967/jnumed.112.105908 PMID: 22915159

29. Innis RB, Cunningham VJ, Delforge J, Fujita M, Gjedde A, Gunn RN, et al. Consensus nomenclature for in vivo imaging of reversibly binding radioligands. J Cereb Blood Flow Metab. 2007; 27: 1533–1539. PMID: 17519979

30. Akaike H. A new look at the statistical model identification. IEEE Trans Auto Cont. 1974; 19: 8.

31. Schwarz G. Estimating the demension of a model. Ann Stat. 1978; 6: 4.

32. Ginovart N, Meyer JH, Boovariwala A, Hussey D, Rabiner EA, Houle S, et al. Positron emission tomography quantification of [11C]-harmine binding to monoamine oxidase-A in the human brain. J Cereb Blood Flow Metab. 2006; 26: 330–344. PMID: 16079787

33. Suhara T, Sudo Y, Okauchi T, Maeda J, Kawabe K, Suzuki K, et al. Extrastriatal dopamine D2 receptor density and affinity in the human brain measured by 3D PET. Int J Neuropsychopharmacol. 1999; 2: 73–82. PMID: 11281973

34. Noguchi J, Zhang MR, Yanamoto K, Nakao R, Suzuki K. In vitro binding of [11C]raclopride with ultra-high specific activity in rat brain determined by homogenate assay and autoradiography. Nucl Med Biol. 2008; 35: 19–27. PMID: 18158939

35. Fujimura Y, Ito H, Takahashi H, Yasuno F, Ikoma Y, Zhang MR, et al. Measurement of dopamine D2 receptors in living human brain using [11C]raclopride with ultra-high specific radioactivity. Nucl Med Biol. 2010; 37: 831–835. doi: 10.1016/j.nucmedbio.2010.04.138 PMID: 20870158

36. Yui J, Hatori A, Kawamura K, Yanamoto K, Yamasaki T, Ogawa M, et al. Visualization of early infarction in rat brain after ischemia using a translocator protein (18 kDa) PET ligand [11C]DAC with ultra-high specific activity. Neuroimage. 2011; 54: 123–130. doi: 10.1016/j.neuroimage.2010.08.010 PMID: 20705143

37. Kawamura K, Kimura Y, Yui J, Wakizaka H, Yamasaki T, Hatori A, et al. PET study using [11C]FTIMD with ultra-high specific activity to evaluate I2-imidazoline receptors binding in rat brains. Nucl Med Biol. 2012; 39: 199–206. doi: 10.1016/j.nucmedbio.2011.07.008 PMID: 21958848

38. Cha JH, Kosinski CM, Kerner JA, Alsdorf SA, Mangiarini L, Davies SW, et al. Altered brain neurotransmitter receptors in transgenic mice expressing a portion of an abnormal human huntington disease gene. Proc Natl Acad Sci U S A. 1998; 95: 6480–6485. PMID: 9600992

39. Yui J, Xie L, Fujinaga M, Yamasaki T, Hatori A, Kumata K, et al. Monitoring neuroprotective effects using positron emission tomography with [11C]ITMM, a radiotracer for metabotropic glutamate 1 receptor. Stroke. 2013; 44: 2567–2572. doi: 10.1161/STROKEAHA.113.001178 PMID: 23908068

40. Kaneda K, Tachibana Y, Imanishi M, Kita H, Shigemoto R, Nambu A, et al. Down-regulation of metabotropic glutamate receptor 1alpha in globus pallidus and substantia nigra of parkinsonian monkeys. Eur J Neurosci. 2005; 22: 3241–3254. PMID: 16367790